Supporting Information

Electrochemical Modeling of Silicon in Lithium-Ion Batteries Using a Multi-Species, Multi-Reaction Framework with Atomistic Insights

Nikolaos Papadopoulos,[1,2,3] Oliver Queisser,[1] Stefanie Arnold,[3] Shubham Dhananjay Bhende[4,5], Jonathan E. Mueller,[4] Simon Schwunk,[1]and Volker Presser[2,3,6,]*

[1] *Dr. Ing. h.c. F. Porsche AG, Porschestraße 911, 71287 Weissach, Germany*

[2] *INM - Leibniz Institute for New Materials, D2 2, 66123, Saarbrücken, Germany*

[3] *Department of Materials Science & Engineering, Saarland University, Campus D2 2, 66123, Saarbrücken, Germany*

[4] *Volkswagen AG, Berliner Ring 2, 38440 Wolfsburg, Germany*

[5] *Faculty of Georesources and Materials Engineering, RWTH Aachen University, Intzestr. 1, 52072 Aachen, Germany*

[6] *saarene, Saarland Center for Energy Materials and Sustainability, Campus C4 2, 66123 Saarbrücken, Germany*

* Corresponding author's email: volker.presser@leibniz-inm.de

1. Further elaboration on the exchange current density at equilibrium

A key implication for the exchange current density at equilibrium conditions (where the net current density is zero) is that the magnitudes of anodic and cathodic current densities must be equal. Consequently, forward and backward reactions continue to occur even at equilibrium, thereby justifying the term dynamic equilibrium.[1] On a macroscopic level, a steady-state is observable without changing concentration. However, on a molecular level, reactants and products are formed and consumed at the same rate between the electrolyte and the active material particles. In the formulation of **Eq. 3** in the manuscript, the active material is treated as an isotropic medium representing a single chemical species.

2. Relation between the regular-solution interaction parameter Ω and electrochemical model parameter w

Starting point is the regular solution theory for a binary mixture desciping the the free energy landscape $g(c_x)$:[2, 3]

$$g(c_x) = -FE^\circ \frac{c_x}{c_{max}} + RT\left[\frac{c_x}{c_{max}}\ln\left(\frac{c_x}{c_{max}}\right) + \left(1-\frac{c_x}{c_{max}}\right)\cdot\ln\left(1-\frac{c_x}{c_{max}}\right)\right] + \Omega\frac{c_x}{c_{max}}\left(1-\frac{c_x}{c_{max}}\right) \quad \textbf{Eq. S1}$$

Here, $\boldsymbol{c_x}$ denotes the lithium concentration, $\boldsymbol{c_{max}}$ the maximum number of available sites with $\boldsymbol{\Omega}$ the regular-solution interaction parameter. The first term expresses the energetic reference of lithium insertion, the logarithmic terms correspond to the ideal configurational entropy of site occupancy, and the final term $\boldsymbol{\Omega\frac{c_x}{c_{max}}\left(1-\frac{c_x}{c_{max}}\right)}$ represents enthalpic interactions between neighbouring species. This framework naturally captures the deviation from ideal mixing that drives phase separation and non-linear voltage behaviour.

The chemical potential is obtained by differentiating **Eq. S1** with respect to $\boldsymbol{c_x}$. The resulting expression **Eq. S2** contains an ideal entropic contribution and an enthalpic correction proportional to $\boldsymbol{\Omega\left(1-2\frac{c_x}{c_{max}}\right)}$, which alters the curvature of the chemical-potential landscape.

$$E_{c_x} = E^\circ + \frac{RT}{F}\ln\left(\frac{c_{max}-c_x}{c_x}\right) - \frac{\Omega}{F}\left(1-2\frac{c_x}{c_{max}}\right) \quad \textbf{Eq. S2}$$

In the main text of this work, non-ideality is represented through a simplified formulation in which the logarithmic term is multiplied by a dimensionless prefactor w:

$$E_{c_x} = E^\circ + w\frac{RT}{F}\ln\left(\frac{c_{max}-c_x}{c_x}\right)$$

3. Atomistic simulation

The numerical data for the potentials presented in **Figure 1B** for crystalline and amorphous electrodes are presented in **Table S1** and **Table S2**. Crystalline and amorphous Li-Si structures shown in **Figure 1C,D** were generated using the workflow described in **Section 5.3** of the manuscript. The crystalline Li-Si model ($Li_{64}Si_{64}$) was obtained by structural optimization toward its lowest-energy configuration, yielding the ordered arrangement characteristic of crystalline Li-Si. In contrast, the amorphous Li-Si model with identical 50:50 stoichiometry was produced through simulated annealing followed by structural relaxation in the Amsterdam Modeling Suite (AMS), resulting in a disordered atomic network that underlies the amorphous voltage response discussed in the main text. In addition to the methodological description provided in the manuscript, **Table S3** summarizes all parameters employed in the ReaxFF simulations, while **Table S4** lists the configuration settings used for the Matlantis calculations.

4. Modell

For the concentration and capacity assignment to each specific material phase ($\mathrm{SiLi^{x}}$), this study adopted an approach introduced by Jiang et al.[4] The maximum Li-Si ratio ($\mathrm{SiLi^{max}}$) is thereby assumed to be 3.7525. However, it is presumed that the capacity of the total 3.75 $\mathrm{SiLi^{max}}$ ratio is shared between $\mathrm{SiLi^{0}}$ and $\mathrm{SiLi^{I}}$ through parameter x**,** whereby 0.0025 stems from a super alloyed $\mathrm{SiLi^{II}}$ and is associated with $c_{\mathrm{max,SiLi^{II}}}$ and $Q_{\mathrm{max,SiLi^{II}}}$**.** The appearance of this super-alloyed phase is interpreted as the formation of critical nuclei that could initiate crystallization if lithiation were extended beyond the applied cutoff potential of 100 mV. In practice, crystallization is expected to occur only at significantly lower potentials, with approximately 50 mV vs. Li/Li^{+} generally considered the threshold for its onset.[4-6] The minor fraction of 0.0025 compared to the total Li/Si ratio of 3.75 explains the comparatively small capacity and maximum concentration values of $\mathrm{SiLi^{II}}$, as shown is **Table 1** and **Table S5**. In the constant-current electrochemical model, x corresponded to 1.32, whereas in the puls-relaxation model, it corresponded to 1.6. The resulting stoichiometries and atomic ratios are summarized in **Table 1** and **Table S5**, respectively. The phase-specific capacities ($Q_{\mathrm{max,SiLi^{x}}}$**)** and concentrations ($c_{\mathrm{max,SiLi^{x}}}$) were calculated using **Eq. S3-S8**.

$$Q_{\mathrm{max,SiLi^0}} = \frac{\mathrm{x}}{3.7525} \cdot Q_{\mathrm{max}} \quad \textbf{Eq. S3}$$

$$Q_{\mathrm{max,SiLi^I}} = \frac{3.75-\mathrm{x}}{3.7525} \cdot Q_{\mathrm{max}} \quad \textbf{Eq. S4}$$

$$Q_{\mathrm{max,SiLi^{II}}} = \frac{0.0025}{3.7525} \cdot Q_{\mathrm{max}} \quad \textbf{Eq. S5}$$

$$c_{\mathrm{max,SiLi^0}} = \frac{Q_{\mathrm{max,SiLi^0}}}{Q_{\mathrm{max}}} \cdot c_{\mathrm{max,SiLi^{max}}} \cdot \mathrm{Si_{util}} \quad \textbf{Eq. S6}$$

$$c_{\mathrm{max,SiLi^I}} = \frac{Q_{\mathrm{max,SiLi^I}}}{Q_{\mathrm{max}}} \cdot c_{\mathrm{max,SiLi^{max}}} \cdot \mathrm{Si_{util}} \quad \textbf{Eq. S7}$$

$$c_{\mathrm{max,SiLi^{II}}} = \frac{Q_{\mathrm{max,SiLi^{II}}}}{Q_{\mathrm{max}}} \cdot c_{\mathrm{max,SiLi^{max}}} \cdot \mathrm{Si_{util}} \quad \textbf{Eq. S8}$$

Since not all lithium sites are expected to be electrochemically active or accessible (Ref.[7]), the parameter $\mathrm{Si_{util}}$ in **Eq. S6-8** denotes the fraction of electrochemical active silicon considered in the simulation (**Table 1** and **Table S5**).

5. Si-electrodes and microstructures

The scanning electron micrographs in **Figure S2** show some conductive graphite (KS6L) of the electrode. Owing to their significantly larger particle size of approximately 1 µm (Ref. [8]) the conductive graphite KS6L is visually well identifiable in electrodes with 10 nm (d_{50}) Si active material. However, it is expected that the distinguishability would vanish in case the particle sizes of KS6L and the active material approach each other in magnitude.

Supporting Tables

Table S1: Atomistic results of stable (gray) and metastable (white) crystalline $SiLi^x$ structures.

CRYSTALLINE STRUCTURES

S. No	Chemical formula	No. Li atoms	No. Si atoms	Total No. of atoms	at% Li	x (Li_xSi)	Matlantis		
							Total energy (eV)	E-formation (eV)	OCP vs.Li/Li^+ (V)
1	Si	0	8	8	0.000	0.000	-36.421	0.000	
2	LiSi	16	16	32	50	1.000	-100.634	-0.067	0.133
3	$Li_{12}Si_7$	96	56	152	63.2	1.714	-445.996	-0.244	0.386
4	Li_7Si_3	84	36	120	70.0	2.333	-329.944	-0.261	0.336
5	Li_5Si_2	15	6	21	71.4	2.500	-57.027	-0.269	0.357
6	$Li_{13}Si_4$	26	8	34	76.5	3.250	-87.130	-0.265	0.245
7	Li_7Si_2	28	8	36	77.8	3.500	-89.259	-0.220	-0.539
8	$Li_{15}Si_4$	60	16	76	78.9	3.750	-188.310	-0.253	0.152
9	$Li_{21}Si_5$	336	80	416	80.8	4.200	-1001.343	-0.236	0.057
10	$Li_{22}Si_5$	352	80	432	81.5	4.400	-1018.960	-0.209	-0.503
11	Li	2	0	2	100	0.000	-3.208	0.000	

Table S2: Atomistic results of stable (gray) and metastable (white) amorphous $SiLi^x$ structures.

AMORPHOUS STRUCTURES

S. No	Chemical formula	No. Li atoms	No. Si atoms	Total No. of atoms	at% Li	x (Li_xSi)	Matlantis		
							Total energy (eV)	E-formation (eV)	OCP vs.Li/Li^+ (V)
1	Si	0	128	128	0	0.000	-554.354	0.000	
2	$LiSi_3$	36	108	144	25.0	0.333	-542.021	-0.119	0.476
3	LiSi	64	64	128	50.0	1.000	-403.049	-0.189	0.379
4	Li_3Si_2	108	72	180	60.0	1.500	-523.364	-0.223	0.355
5	$Li_{12}Si_7$	96	56	152	63.2	1.714	-431.427	-0.240	0.443
6	Li_2Si	108	54	162	66.7	2.000	-444.551	-0.242	0.339
7	Li_7Si_3	168	72	240	70.0	2.333	-632.814	-0.226	0.082
8	Li_5Si_2	135	54	189	71.4	2.500	-492.484	-0.234	0.187
9	$Li_{13}Si_4$	104	32	136	76.5	3.250	-331.910	-0.207	0.082
10	Li_7Si_2	112	32	144	77.8	3.500	-343.697	-0.189	-0.114
11	$Li_{15}Si_4$	120	32	152	78.9	3.750	-356.498	-0.180	0.012
12	$Li_{21}Si_5$	84	20	104	80.8	4.200	-237.826	-0.171	0.011
13	$Li_{22}Si_5$	88	20	108	81.5	4.400	-244.842	-0.171	-1.066
14	Li_5Si	90	18	108	83.3	5.000	-239.266	-0.170	0.163
15	Li	128	0	128	100	6.000	-203.241	0.000	

Table S3: Atomistic simulation specifications and parameters applied in the ReaxFF simulations.

Simulation Parameters – ReaxFF MD	Value / Setting
Force Field	LiSi.ff
Time Step	0.25 fs
Thermostat type	Berendsen
Thermostat damping constant	100 fs
Barostat type	Berendsen
Barostat Pressure / damping constant	1 atm / 500 fs
Barostat Scale	XYZ

Table S4: Atomistic simulation specifications and parameters applied in the Matlantis simulations.

Simulation Parameters – Matlantis	Value / Setting
Optimization Method	FIRE
Convergence Criterion	0.01 eV/Å
Estimator calculator mode	CRYSTAL_U0

Table S5: Electrochemical model parameter set for the pulse-relaxation protocol with 8 h load and 36 h relaxation of a 100-nm-AM Si-Electrode.

Parameter	Model	100 nm Si-Coinzell	Comment/ reference
C/40 current density	±0.595 A/m^2	±0.707 A/m^2	measured
Charge transfer coefficient (α)	0.5		Ref.([4])
Diffusion constant electrolyte (D_l)	2.2-4.2 · 10^{-12} m^2/s		Ref.([9])
Diffusion constant Si (D_s)	1 · 10^{-12} m^2/s		Ref.([9])
Electrode conductivity (σ_s)	20 S/m		assumed
Electrode length	41.3 µm	41.3 µm	measured
Electrode surface (A)		1.13 cm^2	measured
Electrolyte conductivity (σ_l)	0-0.95 S/m		Ref.([9])
Electrolyte Li$^+$ concentration ($c_{\mathrm{l,ref}}$)	1000 mol/m^3	1000 mol/m^3	assumed
Electrolyte transport number (t_+)	0.12-0.37		Ref.([9])
Exchange current density SiLi^0 (j_0^0)	Lith.=0.29; Delith.=0.425 A/m^2		fitted
Exchange current density SiLi^I (j_0^I)	Lith.=0.975; Delith.=0.3512		fitted
Exchange current density $\mathrm{SiLi}^\mathrm{II}$ (j_0^II)	Lith.=0.5; Delith.=1		fitted
Li/Si ratio SiLi^0	0-1.6 (0-62 at% Li)		Figure 1
Li/Si ratio SiLi^I	1.6-3.75 (62-78 at% Li)		Figure 1
Li/Si ratio $\mathrm{SiLi}^\mathrm{II}$	3.75-3.7525 (78-79 at% Li)		Figure 1
Mass Loading Si (m_Si)	1.52 mg/cm^2	1.52 mg/cm^2	measured
Max. capacity (loading)	23810 mAh/m^2		measured
Max. capacity SiLi^0	23279 mAh/m^2		calculated
Max. capacity SiLi^I	31281 mAh/m^2		calculated
Max. capacity $\mathrm{SiLi}^\mathrm{II}$	36.93 mAh/m^2		calculated
Max. Li concentration SiLi^0	118530 mol/m³		calculated
Max. Li concentration SiLi^I	159280 mol/m³		calculated
Max. Li concentration $\mathrm{SiLi}^\mathrm{II}$	185.21 mol/m³		calculated
Max. Li concentration of Si	278000 mol/m³		calculated
Max. Li/Si ratio $\mathrm{SiLi}^\mathrm{max}$	3.7525 (79 at.% Li)		calculated
Molar mass Si (M_Si)	28 g/mol		Ref.([10])
Phase transition parameter (w^0)	Lith.=1.24; Delith.=6.0		fitted
Phase transition parameter (w^I)	Lith.=1.25; Delith.=3.3		fitted
Phase transition parameter (w^II)	Lith.=1; Delith.=3.6		fitted
Porosity (ε_l)	84%	83%	measured
Separator length/thickness	420 µm	420 µm	measured
Si capacity utilization (Si_util)	0.44		calculated
Solid content electrode (ε_s)	16%	17%	calculated
Sphere radius SiLi^x	50 nm	50 nm	assumed
Standard potentials $E^\circ_{\mathrm{SiLi}^0}$	Lith.=375; Delith.=400 (mV)		Figure 1
Standard potentials $E^\circ_{\mathrm{SiLi}^\mathrm{I}}$	Lith.=180; Delith.=275 (mV)		Figure 1
Standard potentials $E^\circ_{\mathrm{SiLi}^\mathrm{II}}$	Lith.=53; Delith.=53 (mV)		Figure 1
Temperature (T)	25 °C	25 °C	measured
Vol.% SiLi^x (Electrode) ($\varepsilon_{\mathrm{s,eff.}}$)	10 %	9.2 %	calculated
Vol.% Binder (Electrode)	3.6 %	4.6 %	calculated
Vol.% Con. Add. (Electrode)	2.4 %	3.2 %	calculated

Supporting Figures

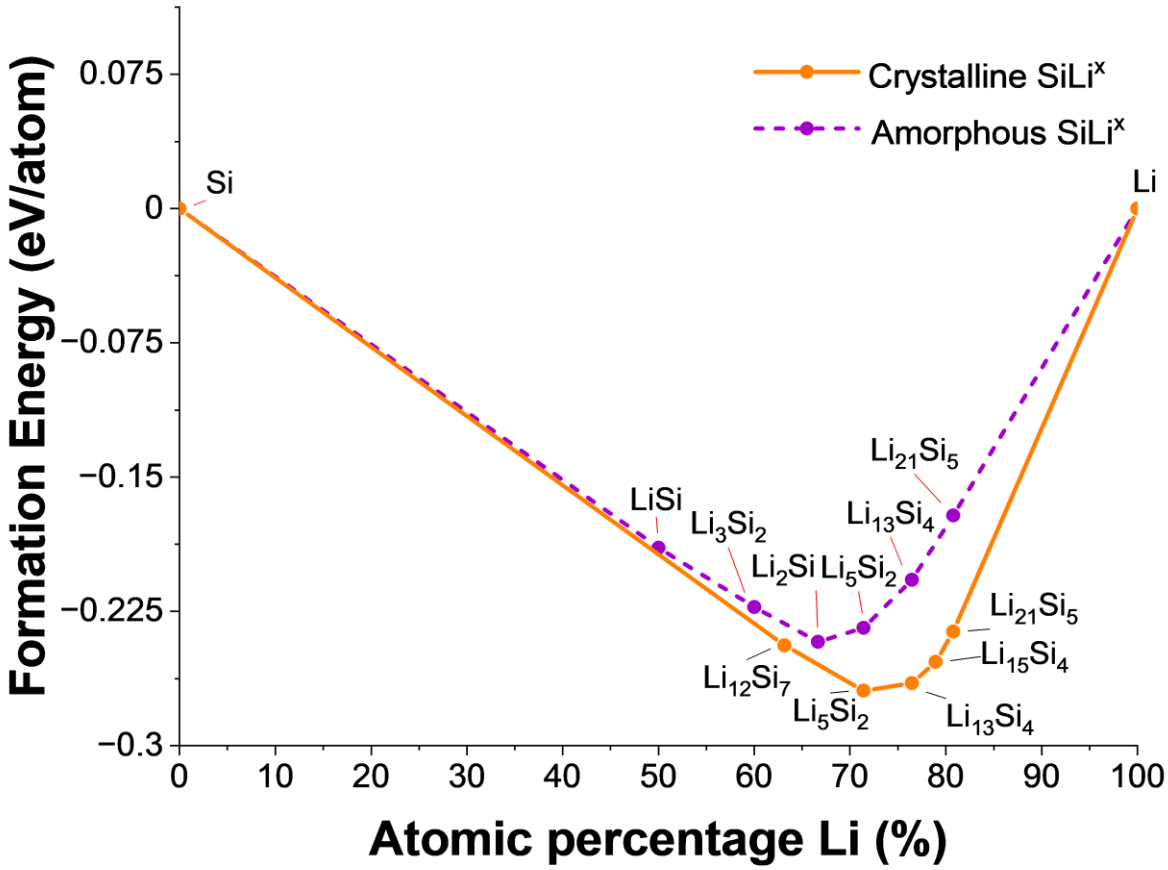

Figure S1: Formation energies of stable crystalline and amorphous Li-Si phases determined from atomistic simulations in this study. Both crystalline (orange) and amorphous (violet) configurations exhibit the characteristic V-shaped formation-energy profile as a function of lithium atomic percentage, consistent with first-principles predictions by Braga et al. (Ref.[11]).

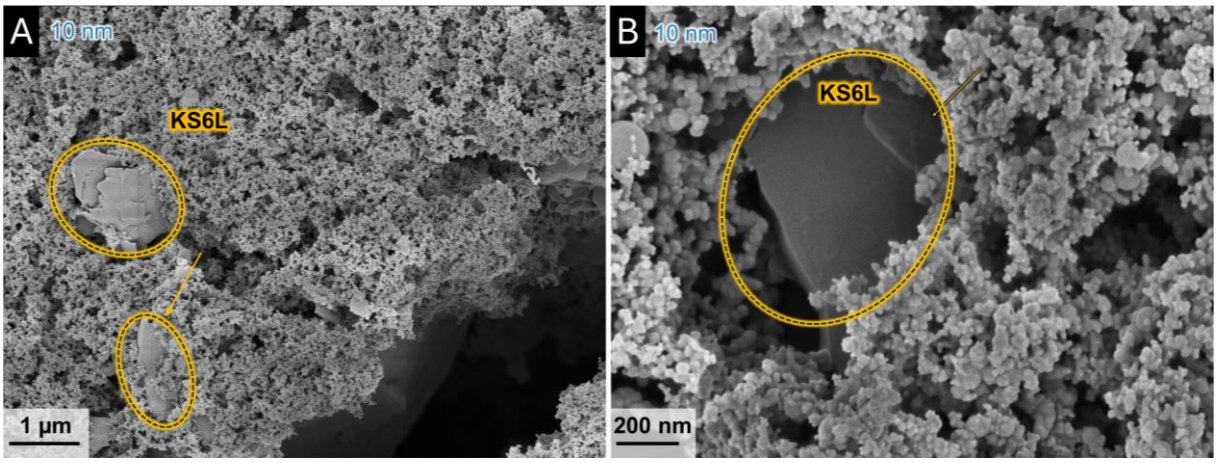

Figure S2: Scanning electron micrographs of silicon electrodes containing 10 nm (d_{50}) active material at different magnifications. (A) Overview image of the electrode surface, revealing the location of conductive graphite particles. (B) Higher-magnification micrograph highlighting the conductive graphite (KS6L) particles, which can be clearly distinguished due to their significantly larger size (~1 µm, Ref. [8]) compared to the surrounding nanoscale silicon particles. The KS6L particles are indicated by yellow dashed outlines.

Supporting References

1. D. R. Baker and M. W. Verbrugge, *Journal of the Electrochemical Society*, 2018, **165**, A3952-A3964.
2. P. Ombrini, M. Z. Bazant, M. Wagemaker and A. Vasileiadis, *npj Computational Materials*, 2023, **9**.
3. P. Ombrini, A. Vasileiadis and M. Wagemaker, *Journal of The Electrochemical Society*, 2025, **172**.
4. Y. Jiang, G. Offer, J. Jiang, M. Marinescu and H. Wang, *Journal of The Electrochemical Society*, 2020, **167**, 130533.
5. W.-J. Zhang, *Journal of Power Sources*, 2011, **196**, 877-885.
6. M. Graf, C. Berg, R. Bernhard, S. Haufe, J. Pfeiffer and H. A. Gasteiger, *Journal of The Electrochemical Society*, 2022, **169**, 020536.
7. C. Berg, R. Morasch, M. Graf and H. A. Gasteiger, *Journal of The Electrochemical Society*, 2023, **170**.
8. K. Pfeifer, S. Arnold, Ö. Budak, X. Luo, V. Presser, H. Ehrenberg and S. Dsoke, *Journal of Materials Chemistry A*, 2020, **8**, 6092-6104.
9. Battery Design Module®. COMSOL Multiphysics® v. 6.3. www.comsol.com. COMSOL AB, Stockholm, Sweden.
10. C. Pereira-Nabais, J. Światowska, A. Chagnes, F. Ozanam, A. Gohier, P. Tran-Van, C.-S. Cojocaru, M. Cassir and P. Marcus, *Applied Surface Science*, 2013, **266**, 5-16.
11. M. H. Braga, A. Dębski and W. Gąsior, *Journal of Alloys and Compounds*, 2014, **616**, 581-593.